Chapter 12
Multi-objective Optimal Reactive Power Dispatch Considering Uncertainties in the Wind Integrated Power Systems

Seyed Masoud Mohseni-Bonab, Abbas Rabiee and Behnam Mohammadi-Ivatloo

Abstract One of the most principle optimization problems which gained the attention of power system operators around the world is optimal power flow (OPF). The OPF basically performs an intelligent power flow and optimizes the system operation condition by optimally determination of control variables. It also considers a specific set of operational constraints and technical limits for this aim, which guaranties both feasibility and optimality of the scheduled operation condition. Generally, this problem can be categorized into two main sub-problems, i.e. optimal reactive power dispatch (ORPD) and optimal real power dispatch, which are differ in their aims and control variables. This chapter deals with the first one, ORPD, which has significant impact on power system security. ORPD is modeled as an optimization problem with nonlinear functions and mixed continuous/discrete variables. Thus, it is a complicated optimization problem. The multi-objective ORPD (MO-ORPD) problem is studied, taking into account different operational constraints such as bus voltage limits, power flow limits of branches, limits of generators voltages, transformers tap ratios and the amount of available reactive power compensation at the weak buses. Three different objective functions are considered in the proposed MO-ORPD framework, which are minimizing total active power losses, minimizing voltage variations and minimizing voltage stability index (*L*-index). These conflicting objectives are optimized via ε-constraint method. In order to model the stochastic behavior of demand and wind power generation, it is necessary to modify the MO-ORPD problem, and develop a probabilistic approach to handle the uncertainties in MO-ORPD problem. Hence, a two-stage stochastic MO-ORPD (SMO-ORPD) is suggested to handle the load and wind power uncertainties in the MO-ORPD problem. In the proposed two-stage

S.M. Mohseni-Bonab · A. Rabiee (✉)
Department of Electrical Engineering, University of Zanjan, Zanjan, Iran
e-mail: rabiee@znu.ac.ir

S.M. Mohseni-Bonab
e-mail: s.m.mohsenibonab@ieee.org; masoud.mohseni-bonab.1@ulaval.ca

B. Mohammadi-Ivatloo
Faculty of Electrical and Computer Engineering, University of Tabriz, Tabriz, Iran
e-mail: mohammadi@ieee.org

N. Mahdavi Tabatabaei et al. (eds.), *Reactive Power Control in AC Power Systems*, Power Systems, DOI 10.1007/978-3-319-51118-4_12

stochastic optimization model, the decision variables are classified into two categories, namely, "*here and now*" and "*wait and see*" variables. The optimal values of "*here and now*" variables should be known before realization of scenarios, and therefore, their values are the same for all scenarios while the optimal values of "*wait and see*" variables are based on the realized scenario, and hence their values are scenario dependent. Moreover, in order to examine performance of the proposed SMO-ORPD and the impact of wind power generation on the results of SMO-ORPD, deterministic ORPD (DMO-ORPD) has also been solved in two modes: DMO-ORPD without wind farms (WFs) and any uncertainty, for the sake of comparison with the available methods in recent literature, and DMO-ORPD with WFs. In this chapter the reactive power compensation devices are modeled as discrete/continuous control variables. DMO-ORPD and SMO-ORPD are formulated as mixed integer non-linear program (MINLP) problems, and solved by General Algebraic Modeling System (GAMS). Also, the IEEE 30-bus standard system is utilized for evaluation of the proposed MO-ORPD models.

12.1 Introduction and Problem Statement

Optimal reactive power dispatch (ORPD) is an important problem for power utilities from the viewpoints of system security and energy losses. ORPD is a specific form of optimal power flow (OPF) problem, in which various objective functions such as transmission losses or voltage stability enhancement indices are optimized by adjusting the generator voltages set-points, reactive power compensation in weak buses and optimal setting of transformers tap ratios.

12.1.1 Background and Review of the Recent Literature

Active power losses are the most important objective function used in the classical OPRD problem. Many heuristic algorithms such as multi-agent-based particle swarm optimization approach (MA-PSO) [1], seeker optimization algorithm (SOA) [2], shuffled frog leaping algorithm (SFLA) and Nelder–Mead SFLA (NM-SFLA) [3], combination of hybrid modified imperialist competitive algorithm (MICA) and invasive weed optimization (IWO) named as (MICA-IWO) [4], combination of modified teaching learning algorithm (MTLA) and double differential evolution (DDE) algorithm [5] have been developed to obtain optimal solutions of ORPD while satisfying technical constraints. In [6], active power losses are minimized in wind farms (WFs) by PSO algorithm taking into consideration the reactive power requirement at the point of common coupling (PCC).

In some papers, active power losses are considered with two other common objective functions of ORPD. At the first category active power losses are considered with voltage deviation, while in the second category active power losses are

optimized along with a voltage stability enhancement index. In the third category active power losses are considered with both of the other objectives. In order to handle these categories, various intelligent algorithms are employed in the existing literature, such as feasible solutions differential evolution (SF-DE), self-adaptive penalty DE (SP-DE), ε-constraint DE (EC-DE) and stochastic ranking DE (SR-DE) in [7], evolutionary programming (EP), PSO, DE and the hybrid differential evolution (HDE) in [8], combination of NM and Firefly Algorithm (FA) in [9], PSO with an aging leader and challengers (ALC-PSO) in [10] and gray wolf optimizer (GWO) in [11], linear programming (LP) based method using FACTS devices in [12], nonlinear programming (NLP) based method for optimizing local voltage stability index in [13], SOA in [14], DE in [15], PSO, simple genetic algorithm (SGA) and harmony search algorithm (HSA) in [16], gravitational search algorithm (GSA) in [17].

A different research carried out on the single objective ORPD problem, in which steady state voltage stability analysis has been carried out in [18] considering initial conditions for transient stability (TS), small disturbance (SD), and continuation power flow (CPF) for minimizing real power losses. Also, penalty function based method has been presented in [19] to convert discrete ORPD model to a continuous and differentiable model.

The multi-objective ORPD (MO-ORPD) has attracted the attention researchers in recent years. Similar to single objective OPRD, many algorithms utilized to deal with MO-ORPD by considering two or three objective conflicting functions, simultaneously. Most popular objective function of MO-ORPD problem is real power losses which is considered with voltage deviation (as the conflicting objective function) in [20], and solved by strength Pareto evolutionary algorithm (SPEA). Also, it is solved in [21] by non-dominated sorting genetic algorithm-II (NSGA-II).

MO-ORPD problem is modeled as a mixed integer nonlinear program (MINLP) and solved in some literature with considering real power losses and $L_{\max}$ index. It is worth to note that, $L_{\max}$ is a voltage stability index, where it varies from 0 at no-load condition to 1 at voltage collapse point. In [22], NSGA-II and modified NSGA-II (MNSGA-II), In [23] hybrid fuzzy multi-objective evolutionary algorithm (HFMOEA) and in [24], chaotic improved PSO based multi-objective optimization (MOCIPSO) and improved PSO-based multi-objective optimization (MOIPSO) are used for this aim. In more advanced MO-ORPD problem, three objective functions are considered simultaneously. For instance, teaching learning based optimization (TLBO) and quasi-oppositional TLBO (QOTLBO) in [25], chaotic parallel vector evaluated interactive honey bee mating optimization (CPVEIHBMO) in [26], and strength Pareto multi-group search optimizer (SPMGSO) [27] are used to solve MO-ORPD problem.

Moreover, in recent literature ORPD or MO-ORPD problems are solved considering the effects of technical uncertainties raised from the power system restructuring, probable disturbances, or the integration of renewable energies. In [28], chance constrained programming technique is proposed to solve ORPD problem with the aim of minimizing active power losses. Nodal power injections and random branch outages are considered as uncertainty sources. In [29, 30]

the load uncertainty is included in MO-ORPD problem, considering different objective functions. Monte Carlo simulations (MCS) are used for handling the load uncertainties in the nonlinear constrained multi objective ORPD problem.

12.1.2 Chapter Contributions

The main focus of this chapter is to solve the MO-ORPD problem in a wind integrated power system considering the uncertainties of load demand and wind power generation. Even these two sources of uncertainty are considered here, but the proposed method is generic and other uncertainty sources could be included via the proposed scenario based approach. The normal probability distribution function (PDF) and Rayleigh (PDF) are used for modeling the load and wind speed uncertainties, respectively.

Three different objective functions, namely active power losses, voltage stability index ($L_{\max}$), and voltage deviations at load buses are considered. The multi-objective problem is handled using ε-constraint technique and optimal Pareto sets are obtained for each pair of the above objective functions. In this chapter, for the sake of comparison with existing methods, the reactive power compensation by shunt VAR compensators is modeled as continuous variable in deterministic MO-ORPD (DMO-ORPD), while in real world problems discrete model is employed for these devices in the proposed stochastic MO-ORPD (SMO-ORPD). Thus, the DMO-ORPD is a NLP problem, while the SMO-ORPD is a MINLP problem. The proposed optimization problems are implemented in GAMS [31], and solved by SNOPT [32] and SBB [33] solvers, for NLP and MINLP problems, respectively.

Hence, the main contributions of this chapter are outlined as follows:

- Modeling and including stochastic nature of loads and wind power generations in the MO-ORPD problem (i.e. development of SMO-ORPD problem).
- Investigation of the impact of renewable power generation on the results obtained by ORPD problem.
- Utilizing discrete model for shunt VAR compensation devices in the proposed SMO-ORPD problem, since most of the pervious literature used continuous modeling for capacitor banks.
- Implementation of ε-constraint technique and fuzzy satisfying criteria to solve the MO-ORPD problem, and for selection of the best compromise solution, respectively.
- Providing comprehensive illustrative studies for different types of ORPD problem, such as DMO-ORPD with and without wind integration and SMO-ORPD.
- Comparison of the obtained results for DMO-ORPD case with previously published methods in literature, which confirms the efficiency of the proposed method.

12.2 Uncertainty Modeling

Uncertain parameters in power systems are classified to technical and economical parameters. Technical parameters consist of operational (like demand and generation) and topological parameters, whereas economical parameters include macroeconomic and microeconomic parameters [34]. There are different methods for modeling these uncertain parameters which are summarized in Fig. 12.1. In this chapter, scenario based probabilistic method is utilized to handle to uncertainties. At the following, the detailed description of considered scenarios is given.

12.2.1 Demand Uncertainty Characterization via Scenario Based Modeling

On account of stochastic nature of the load demand in electric power systems, it is required to model the load uncertainty in operation and planning of power systems. In the general manner load uncertainty can be modeled using the normal or Gaussian PDF [35]. In this chapter, it is presumed that the mean and standard deviation of the load PDF, μ_D and σ_D are known. Probability of d-th load scenario is represented by π_d (probability of demand scenario d) and calculated using (12.1). Figure 12.2 shows the load levels. It is worth to note that $P_{D_d}^{\min}$ and $P_{D_d}^{\max}$ (minimum/maximum value of real power demand at d-th load scenario) are the boundaries of d-th interval (or d-th load scenario), as shown in Fig. 12.2.

$$\pi_d = \int_{P_{D_d}^{\min}}^{P_{D_d}^{\max}} \frac{1}{\sqrt{2\pi\sigma^2}} \exp\left[-\frac{(P_D - \mu_D)^2}{2\sigma^2}\right] dP_D \tag{12.1}$$

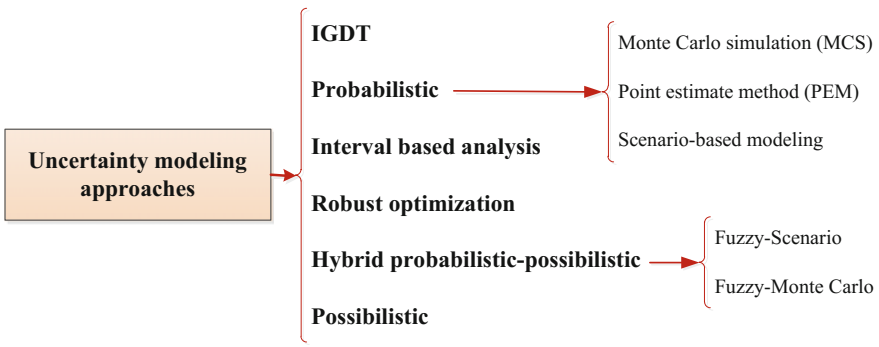

Fig. 12.1 Uncertainty modeling approaches [34]

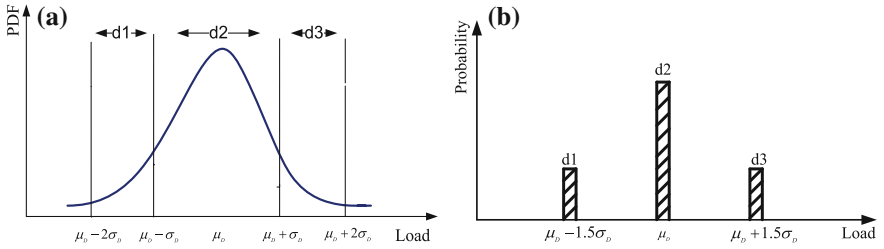

Fig. 12.2 The load PDF and load scenarios, **a** Normal PDF, **b** considered scenarios

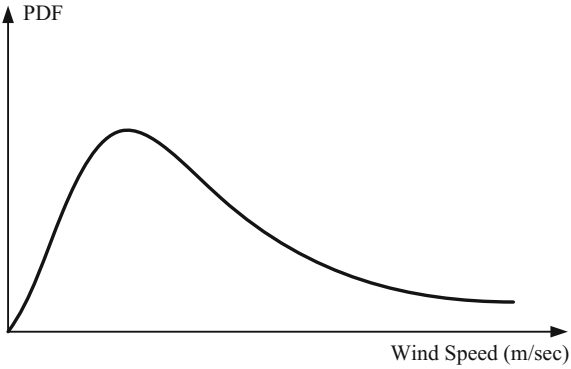

Fig. 12.3 Rayleigh PDF for wind speed characterization

$$P_{D_d} = \frac{1}{\pi_d} \int_{P_{D,d}^{\min}}^{P_{D,d}^{\max}} \left(P_D \times \frac{1}{\sqrt{2\pi\sigma^2}} \exp\left[-\frac{(P_D - \mu_D)^2}{2\sigma^2} \right] \right) dP_D \tag{12.2}$$

12.2.2 Wind Power Generation Uncertainty Modeling

Principally the wind speed uncertainty is modeled using the Rayleigh or Weibul PDF [36, 37]. It should be noticed that the Weibull distribution is a generalized form of the Rayleigh PDF. The Rayleigh PDF of the wind speed which is depicted in Fig. 12.3, can be exhibited as follows

$$\mathrm{PDF}(v) = \left(\frac{v}{c^2} \right) \exp\left[-\left(\frac{v}{\sqrt{2}c} \right)^2 \right] \tag{12.3}$$

where v is wind speed in m/s.

The wind speed variation range is classified into intervals, which is named wind scenarios. The probability of each scenario can be calculated from the following equation. The probability of scenario s and the corresponding wind speed v_s is calculated using the following equations.

$$\pi_w = \int_{v_{i,w}}^{v_{f,w}} \left(\frac{v}{c^2}\right) \exp\left[-\left(\frac{v}{\sqrt{2}c}\right)^2\right] dv \tag{12.4}$$

$$v_w = \frac{1}{\pi_w} \int_{v_{i,w}}^{v_{f,w}} \left(v \times \left(\frac{v}{c^2}\right) \exp\left[-\left(\frac{v}{\sqrt{2}c}\right)^2\right]\right) dv \tag{12.5}$$

where, v_w is the wind speed at w-th wind scenario, and $v_{i,w}, v_{f,w}$ are the starting and the last points of wind speed's interval at w-th scenario, respectively. Also, c is scaling parameter which is acquired by historical wind data.

The characteristics curve of a wind turbine determines the correspondence between the available wind speed and generated wind power. A linearized characteristics curve is presented in Fig. 12.4 [38]. Using this curve, the predicted production power of the wind turbine for various wind speeds can be obtained using the following equation.

$$P_w^{avl} = \begin{cases} 0 & v_w \le v_{in}^c \text{ or } v_w \ge v_{out}^c \\ \frac{v_w - v_{in}^c}{v_{rated} - v_{in}^c} P_r^w & v_{in}^c \le v_w \le v_{rated} \\ P_r^w & v_{rated} \le v_w \le v_{out}^c \end{cases} \tag{12.6}$$

where, P_w^{avl} is available wind power generation, v_{in}^c, v_{out}^c are cut-in/out speed of wind turbine in m/s, and v_{rated} is rated speed of wind turbine in m/s.

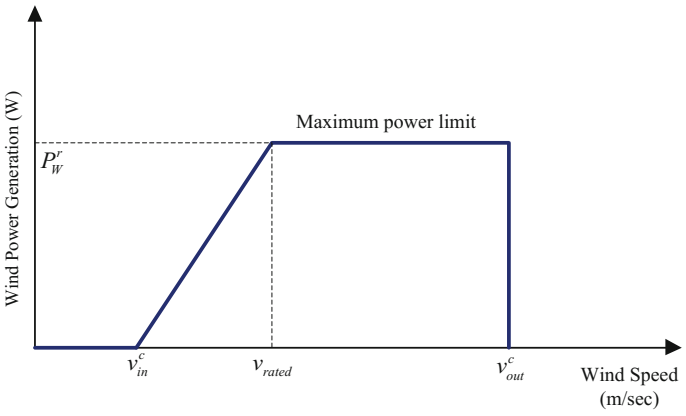

Fig. 12.4 The power curve of a wind turbine

By producing the appropriate number of scenarios for wind power and load demand, the whole number of compound wind-load scenarios is attained by multiplying the number of wind and load individual scenarios. The probability of scenario s, which is acquired considering w-th scenario of wind and d-th scenario of load demand, can be attained using the following equation.

$$\pi_s = \pi_w \times \pi_d \tag{12.7}$$

where, π_s is probability of scenario s, and π_w is probability of wind power generation scenario w.

Figure 12.5 illustrates the procedure used to generate the total number of 15 wind-load scenarios with related probabilities. As presented in Fig. 12.5, the normal probability distribution function (PDF) and Rayleigh (PDF) are used for modeling the load and wind speed uncertainties. The mean value of this PDF is the rated power of loads given in [39]. The standard deviation is supposed to be 2% of the mean load. Also, the entire PDF of loads is divided into three discrete areas and hence three scenarios are considered for loads. The parameters of wind speed PDF and the correlating wind power generation scenarios for this wind farm are adjusted from [40]. There are five wind power generation scenarios, which their features are summarized in Fig. 12.5.

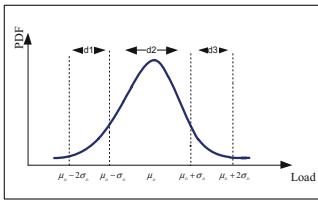

load scenarios

	Load (%)	π_d
d_1	97	0.15
d_2	100	0.7
d_3	103	0.15

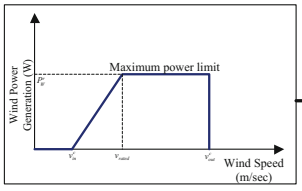

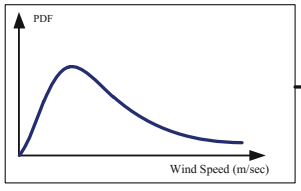

Wind power generation scenarios

	Wind (%)	π_w
w_1	0	0.0689
w_2	12.87	0.2044
w_3	49.37	0.4048
w_4	86.83	0.1992
w_5	100	0.1227

Scenario Number	Load (%)	Wind (%)	π_s
s_1	97	0	0.010335
s_2	97	12.87	0.03066
s_3	97	49.37	0.06072
s_4	97	86.83	0.02988
s_5	97	100	0.018405
s_6	100	0	0.04823
s_7	100	12.87	0.14308
s_8	100	49.37	0.28336
s_9	100	86.83	0.13944
s_{10}	100	100	0.08589
s_{11}	103	0	0.010335
s_{12}	103	12.87	0.03066
s_{13}	103	49.37	0.06072
s_{14}	103	86.83	0.02988
s_{15}	103	100	0.018405

Fig. 12.5 Illustration of scenario generation procedure

12.3 The Problem Formulation

In this section, the studied objective functions, description of ε-constraint method for dealing with the MO-ORPD, fuzzy satisfaction method for selection of the best compromise solution, and the operational constraints such as load flow equations along with various technical limits, are represented.

12.3.1 Objective Functions

Voltage stability of the power system is greatly related to reactive power management. Hence, voltage stability improvement is also considered as another objective function along with the total active power losses and voltage deviations. These objective functions may be conflicted [2, 24]. The subsets of ORPD problem variables can be stated as follows.

$$\bar{\Theta} = \begin{bmatrix} V_{i,} & \forall i \in \Omega_G \\ t_m, & \forall m \in \Omega_T \\ Q_{C_i,s}, & \forall i \in \Omega_C, \ \forall s \in \Omega_S \\ P_{W_i,s}, & \forall i \in \Omega_W, \ \forall s \in \Omega_S \\ Q_{W_i,s}, & \forall i \in \Omega_W, \ \forall s \in \Omega_S \end{bmatrix}$$
$$\bar{X} = \begin{bmatrix} V_{i,s}, & \forall i \in \Omega_{PQ}, \ \forall s \in \Omega_S \\ \theta_{i,s}, & \forall i \in \Omega_B, \ \forall s \in \Omega_S \\ S_{\ell,s}, & \forall \ell \in \Omega_L, \ \forall s \in \Omega_S \\ Q_{G_i,s}, & \forall i \in \Omega_G, \ \forall s \in \Omega_S \\ P_{G_i,s}, & \forall i = sb, \ \forall s \in \Omega_S \end{bmatrix} \tag{12.8}$$

where, $\overline{\Theta}$ is vector of control variables, $\overline{X}$ is vector of state (or dependent) variables, Ω_B is set of all buses, Ω_L is set of all branches, Ω_G is set of all generating units, Ω_W is set of wind farms, Ω_S is set of all possible scenarios, Ω_T is set of all tap changing transformers, Ω_C is set of all VAR compensators, Ω_{PQ} is set of system PQ buses, and Ω_{B_i} is set of buses connected to bus i.

12.3.1.1 Minimization of Total Active Power Losses

Minimizing the total power losses in transmission system is critical objective in power systems for improvement of the total energy efficiency and economic reasons. The active power losses in scenario s is mathematically expressed as follows.

$$PL_s\left(\overline{\Theta}_s, \overline{X}_s\right) = \sum_{i\in\Omega_G} P_{G_i,s} + \sum_{i\in\Omega_W} P_{W_i,s} - \sum_{i\in\Omega_B} P_{D_i,s} \tag{12.9}$$

where, PL_s is active power losses in scenario s, $P_{G_i,s}$ is active power production of generator at bus i in scenario s, $P_{W_i,s}$ active power generation of wind farm at scenario s, and $P_{D_i,s}$ real power demand of i-th bus in scenario s.

Expected value of power losses (EPL), Ξ_{PL}, over the whole scenarios is considered as the first objective function, F_1. It is computed using the following equation.

$$F_1 = \Xi_{PL} = \sum_{s\in\Omega_S} (\pi_s \times PL_s) \tag{12.10}$$

where, $\Xi_{PL}^{\min}/\Xi_{PL}^{\max}$ are minimum/maximum value for expected real power loss.

12.3.1.2 Minimization of Voltage Deviations

The second objective of ORPD problem is to sustain a proper voltage level at load buses. Electrical equipment is constructed for optimal operation of nominal voltage. Any violation from this rated voltage can result in reduced efficiency and life reduction of electric devices. Thus, the voltage profile of the system could be optimized by minimization of the total voltage deviations (VD) from the corresponding rated values at load buses. This objective function is represented as follows.

$$VD_s\left(\overline{\Theta}_s, \overline{X}_s\right) = \sum_{i\in\Omega_{PV}} \left|V_{i,s} - V_{i,s}^{spc}\right| \tag{12.11}$$

where, VD_s is voltage deviations value in scenario s, $V_{i,s}$ is voltage magnitude of bus i in scenario s, and Ω_{PV} is set of system PV buses.

Similar to the F_1, here, the expected value of voltage deviations (EVD), Ξ_{VD}, is the second conflicting objective function (F_2). EVD is calculated as follows.

$$F_2 = \Xi_{VD} = \sum_{s\in\Omega_S} (\pi_s \times VD_s) \tag{12.12}$$

where, $\Xi_{VD}^{\min}/\Xi_{VD}^{\max}$ are minimum/maximum value of expected voltage deviation.

12.3.1.3 Minimization of Voltage Stability Index (L-Index)

Some methods can be used for associating static voltage stability enhancement in ORPD problem. For example, power-voltage curves is utilized as an index in [41]

for static voltage stability modeling. Static voltage stability index based on the modal analysis was used in [42] for determination of voltage stability margin. Minimum singular value of the load flow Jacobin matrix [43] and minimum *L*-index [44] are other indexes used for determining the voltage stability margin of the system. In this chapter *L*-index is selected for quantifying voltage stability. This index illustrates the distance of the current state of power system from the voltage stability limit point, which is evaluated using power flow solution. It should be mentioned that the value of *L*-index varies between 0 and 1. *L*-index value less than 1 (voltage collapse point) and close to 0 (no load point) corresponds with more voltage stability margin. The voltage magnitude and phase angle of network buses are functions of system load and generation. By enlarging the transmitted power and for near maximum power transfer position, the voltage stability index values for load buses becomes closer to 1, which shows that the system is closer to voltage collapse. For any load node *j*, *L*-index can be expressed as [25]

$$L_j = \left| 1 - \sum_{i \in \Omega_G} \overline{\lambda}_{ji} \frac{\overline{V}_i}{\overline{V}_j} \right|, \quad \forall j \in \Omega_{PQ} \tag{12.13}$$

where, $\overline{V}_i = V_i \angle \delta_i$ and $\overline{V}_j = V_j \angle \delta_j$. In order to calculate $\overline{\lambda}_{ji}$, the system Y_{BUS} matrix is reorganized as follows

$$\begin{bmatrix} \overline{I}_L \\ \overline{I}_G \end{bmatrix} = \begin{bmatrix} Y_{GG} & Y_{GL} \\ Y_{LG} & Y_{LL} \end{bmatrix} \begin{bmatrix} \overline{V}_L \\ \overline{V}_G \end{bmatrix} \tag{12.14}$$

where $\overline{V}_L$ and $\overline{I}_L$ are the vectors of *PQ* buses voltage and injected currents phasors, whereas $\overline{V}_G$ and $\overline{I}_G$ are the ones for generator buses (including slack and *PV* buses). Since, $\overline{I}_L = 0$, the following expression can be inferred from (12.14).

$$\overline{\Gamma} = -[Y_{LL}]^{-1}[Y_{LG}] \tag{12.15}$$

Since $\overline{\Gamma}$ is a complex matrix, then $\overline{\lambda}_{ji}$ in (12.13) can be obtained as follows.

$$\overline{\Gamma} = \left[\overline{\lambda}_{ji}\right], (\forall j \in \Omega_{PQ}, \forall i \in \Omega_G) \tag{12.16}$$

where, *i*, *j* are indexes of bus numbers.

Therefore, for each scenario *s*, the maximum value of *L*-index among all load buses is considered as the voltage stability index as follows

$$LM_s\left(\overline{\Theta}_s, \overline{X}_s\right) = \max(L_j), \forall j \in \Omega_{PQ} \tag{12.17}$$

where, LM_s is $L_{\max}$ value in scenario *s*.

The third objective (F_3) is the expected value of $L_{\max}$, Ξ_{LM}, for all scenarios, which is obtained as follows

$$F_3 = \Xi_{LM} = \sum_{s \in \Omega_S} (\pi_s \times LM_s) \tag{12.18}$$

where, $\Xi_{LM}^{\min}/\Xi_{LM}^{\max}$ are minimum/maximum value of $EL_{\max}$.

12.3.2 ε-Constraint Method

ε-constraint method is an approach in which the multi-objective optimization problem is converted to a conventional single-objective problem [35]. In this method, all objective functions except one, considered as inequality constraints by assigning a proper value of control parameter named as ε parameter. In the proposed SMO-ORPD problem, two different multi-objective cases are studied.

In the first case (Case-I), F_1 and F_2 are minimized. In order to solve this multi-objective optimization problem by ε-constraint method, one of the objective functions (here we assumed F_2) is moved to the constraints, i.e. it is considered as a constraint and the other objective (here, F_1) is minimized subject to this new constraint and the constraints of the original multi-objective problem, as follows.

$$\begin{aligned} &\min\ (F_1) \\ &\text{s.t.: } F_2 \leq \varepsilon_{F_2} \end{aligned} \tag{12.19}$$

It can be observed from (12.19) that Ξ_{VD} is constrained by the parameter ε. This parameter varies from the minimum value to the maximum value of F_2 (from $F_2^{\min}$ to F_2^{max}) and F_3 (from $F_3^{\min}$ to $F_3^{\max}$) gradually, and for any value of ε_{F_2} the modified single objective optimization problem (12.19) is solved. The set of obtained solutions for the entire variations of ε_{F_2} are called Pareto optimal front of the multi-objective optimization problem.

Similarly, in the second case (Case-II), F_1 and F_3 are minimized. In the ε-constraint method, one of the objectives (here F_3) is moved to the constraints, i.e. it is considered as a constraint and the other objective (F_1) is minimized subject to this new constraint and the constraints of the original multi-objective problem, as follows.

$$\begin{aligned} &\min(F_1) \\ &\text{s.t. :} \quad F_3 \leq \varepsilon_{F_3} \end{aligned} \tag{12.20}$$

Similarly, in this case Ξ_{LM} is constrained by the parameter ε_{F_3}. This parameter varies from the minimum value to the maximum value of F_3 (from $F_3^{\min}$ to F_3^{max})

gradually, and for any value of ε_{F_3} the modified single objective optimization problem (12.20) is solved and the Pareto optimal front of the problem is obtained.

12.3.3 Fuzzy Decision Maker

By solving the MO-ORPD problem a Pareto front is derived. The solutions corresponding to Pareto front are non-dominated solution and another method is required to select the best compromising solution among the obtained non-dominated solutions. Fuzzy decision maker is utilized in this chapter for this purpose. In this method a fuzzy membership function is assigned to each solution in the Pareto front. The fuzzy membership is in the interval [0, 1]. The linear fuzzy membership functions can be expressed for k-th objective function using the following equation [35].

$$\mu_k = \begin{cases} 1 & F_k \le F_k^{\min} \\ \frac{F_k - F_k^{\max}}{F_k^{\min} - F_k^{\max}} & F_k^{\min} \le F_k \le F_k^{\max} \\ 0 & F_k \ge F_k^{\max} \end{cases} \tag{12.21}$$

where, k is index of objective functions, F_k is individual value of k-th conflicting objective function and $\hat{F}_k$ is normalized value of k-th objective function.

For the obtained Pareto optimal set, the best compromise solution can be selected using the min-max method described in [45]. In this method, for r-th Pareto optimal solution the minimum membership number $(\hat{\mu}_r)$ is obtained as follows:

$$\hat{\mu}_r = \min(\mu_k), \forall k \in \Omega_{OF} \tag{12.22}$$

where, Ω_{OF} is set of conflicting objective functions.

Now, the best compromise solution is that which has the maximum value of minimum membership number, as follows:

$$\widehat{\mu} = \max(\hat{\mu}_r), \forall r \in \Omega_{POS} \tag{12.23}$$

where, Ω_{POS} is set of all optimal Pareto solutions of a multi-objective optimization problem.

12.3.4 Constraints

12.3.4.1 Equality Constraints (AC Power Balance Equations)

The feasible solution should assure the power flow equations in each scenario, which are represented mathematically in the following.

$$\begin{cases} P_{G_i,s} + P_{W_i,s} - P_{D_i,s} = \sum\limits_{j \in \Omega_{B_i}} V_{i,s} V_{j,s} \left(G_{ij} \cos\left(\theta_{i,s} - \theta_{j,s}\right) + B_{ij} \sin\left(\theta_{i,s} - \theta_{j,s}\right) \right) \\ Q_{G_i,s} + Q_{W_i,s} + Q_{C_i,s} - Q_{D_i,s} = \sum\limits_{j \in \Omega_{B_i}} V_{i,s} V_{j,s} \left(G_{ij} \sin\left(\theta_{i,s} - \theta_{j,s}\right) - B_{ij} \cos\left(\theta_{i,s} - \theta_{j,s}\right) \right) \end{cases} \tag{12.24}$$

where, $P_{G_i,s}, Q_{G_i,s}$ are active and reactive powers production of generator at bus i in scenario s, $P_{W_i,s}, Q_{W_i,s}$ active and reactive power generations of wind farm at scenario s, $P_{D_i,s}, Q_{D_i,s}$ real and reactive power demand of i-th bus in scenario s, and G_{ij}, B_{ij} are real and imaginary parts of ij-th element of Y_{BUS} matrix (pu/radian).

12.3.4.2 Inequality Constraints

The active and reactive power output of generators and voltage magnitudes of all buses should be kept in the predefined ranges as follows.

$$P_{G_i}^{\min} \leq P_{G_{sl},s} \leq P_{G_i}^{\max}, \forall i = sb, \forall s \in \Omega_S \tag{12.25}$$

$$Q_{G_i}^{\min} \leq Q_{G_i,s} \leq Q_{G_i}^{\max}, \forall i \in \Omega_G, \forall s \in \Omega_S \tag{12.26}$$

$$V_i^{\min} \leq V_{i,s} \leq V_i^{\max}, \forall i \in \Omega_B, \forall s \in \Omega_S \tag{12.27}$$

where, $P_{G_i}^{\min}, P_{G_i}^{\max}$ are minimum and maximum value for active power, $Q_{G_i}^{\min}, Q_{G_i}^{\max}$ are minimum and maximum value for reactive power of generator at bus i, and $V_i^{\min}/V_i^{\max}$ are minimum and maximum value for voltage magnitude of i-th bus.

The power flowing from the branches is constrained to its maximum value as follows.

$$\left|S_{\ell,s}\right| \leq S_{\ell}^{\max}, \forall \ell \in \Omega_L, \forall s \in \Omega_S \tag{12.28}$$

where, ℓ is index of transmission lines, $S_{\ell,s}$ is power flow of ℓ - th branch in scenario s, and $S_{\ell}^{\max}$ is maximum transfer capacity of line ℓ.

The tap amounts of tap changers are also restricted as follows.

$$t_m^{\min} \leq t_m \leq t_m^{\max}, \forall m \in \Omega_T \tag{12.29}$$

where, m is index of tap changing transformers, and $t_m^{\min}, t_m^{\max}$ are minimum/maximum value for m-th tap changer.

It is noteworthy that the reactive power output of VAR compensation devices are modeled as a multi-step compensation, i.e. a discrete variable is utilized for each VAR compensation node as follows, which determines the required steps for VAR injections.

$$Q_{C_i,s} = Q_{C_i}^{b} \times u_{C_i,s}, \forall i \in \Omega_C, \forall s \in \Omega_S \tag{12.30}$$

where, $Q_{C_i,s}$ is reactive power compensation at bus i in scenario s, $Q_{C_i}^{b}$ is VAR compensation capacity in each step at bus i, and $u_{C_i,s}$ is reactive power compensation step at bus i in scenario s.

The reactive power compensation stages are restricted as follows

$$u_{C_i}^{\min} \le u_{C_i,s} \le u_{C_i}^{\max} \quad \forall i \in \Omega_C, \forall s \in \Omega_S \tag{12.31}$$

where, $u_{C_i}^{\min}, u_{C_i}^{\max}$ are minimum and maximum value for reactive power compensation at bus i.

Also, for the available active and reactive power outputs of wind farms, the following constraints should be satisfied

$$0 \le P_{W_i,s} \le \zeta_{W_{i,s}} \times P_{W_i}^{r}, \forall i \in \Omega_W, \forall s \in \Omega_S \tag{12.32}$$

$$Q_{W_i}^{\min} \le Q_{W_i,s} \le Q_{W_i}^{\max}, \forall i \in \Omega_W, \forall s \in \Omega_S \tag{12.33}$$

where, $P_{W_i}^{r}$ is wind farm rated capacity installed in bus i, $\zeta_{W_{i,s}}$ is percentage of wind power rated capacity realized at scenario s in bus i, and $Q_{W_i}^{\min}, Q_{W_i}^{\max}$ are minimum/maximum value of reactive power produced by wind farm.

In this chapter in line with references [35–37], the reactive power output of wind farms are related to the active power output as follows.

$$\begin{cases} Q_{W_i}^{\max} = \tan\left(\cos^{-1}(PF_{lg,i})\right) \times P_{W_i,s} \\ Q_{W_i}^{\min} = -\tan\left(\cos^{-1}(PF_{ld,i})\right) \times P_{W_i,s} \end{cases} \tag{12.34}$$

where, $PF_{lg,i}, PF_{ld,i}$ are lag/lead power factor limits of the wind farms located at node i.

12.4 Scenario Generation and Two-Stage Stochastic Programming

In this chapter two-stage stochastic programming method is utilized for decision making in an uncertain environment. In this method, the decision variables are classified as "*here and now*" and "*wait and see*" variables [46]. The optimal values of "*here and now*" or *"first stage"* variables should be recognized before realization of scenarios. In other words, their values are scenario independent and are similar for all scenarios. In other words, the optimal values of "*wait and see*" or *"second stage"* variables should be considered after realization of the scenarios. In other words, their values are scenario dependent and may be different for different

scenarios. In the suggested SMO-ORPD problem the decision variables (DVs) are generator voltages, tap values of tap changing transformers and reactive power output of VAR compensators in the weak buses.

As it is mentioned before, the set of control variables is categorized into two separated subsets, i.e. *here and now* and *wait and see* control variables. The set of here and now decision variables (DV_{HN}) are as follows:

$$DV_{HN} = \left\{ \begin{matrix} V_i, & \forall i \in \Omega_G \\ t_m, & \forall m \in \Omega_T \end{matrix} \right\} \tag{12.35}$$

where, t_m is value of m-th tap changer setting.

Also, the set of wait and see decision variables (DV_{WS}) are as follows.

$$D_{WS} = \left\{ \begin{matrix} Q_{C_i,s}, & \forall i \in \Omega_C, & \forall s \in \Omega_S \\ P_{W_i,s}, & \forall i \in \Omega_W, & \forall s \in \Omega_S \\ Q_{W_i,s,} & \forall i \in \Omega_W, & \forall s \in \Omega_S \end{matrix} \right\} \tag{12.36}$$

where, $Q_{C_i,s}$ is reactive power compensation at bus i in scenario s.

12.5 Simulations on a Standard Test System

Simulations are carried out on the IEEE 30-bus test system. In order to show the effectiveness of the presented approach, several cases are studied as follows.

(A) Deterministic optimization without wind farms (by neglecting the uncertainties of load and wind farms)
(B) Deterministic optimization with the expected value of wind farms power output and mean value of load (by neglecting uncertainty)
(C) Stochastic optimization with load and wind farms power generation uncertainties (uncertainty representation using scenario based approach).

For the sake of comparison with available methods in literature, the VAR compensation devices are modeled as continuous control variables in case (A). While in cases (B) and (C) the VAR compensations are modeled with discrete steps as defined in previous section.

In cases (B) and (C), it is assumed that a wind farm with 56 MW rated capacity is installed at bus 20.

12.5.1 Test System

IEEE 30-bus system [47] includes 30 buses with 6 generator buses as represented in Fig. 12.6. Bus 1 is the slack bus and buses 2, 5, 8, 11 and 13 are *PV* buses whereas

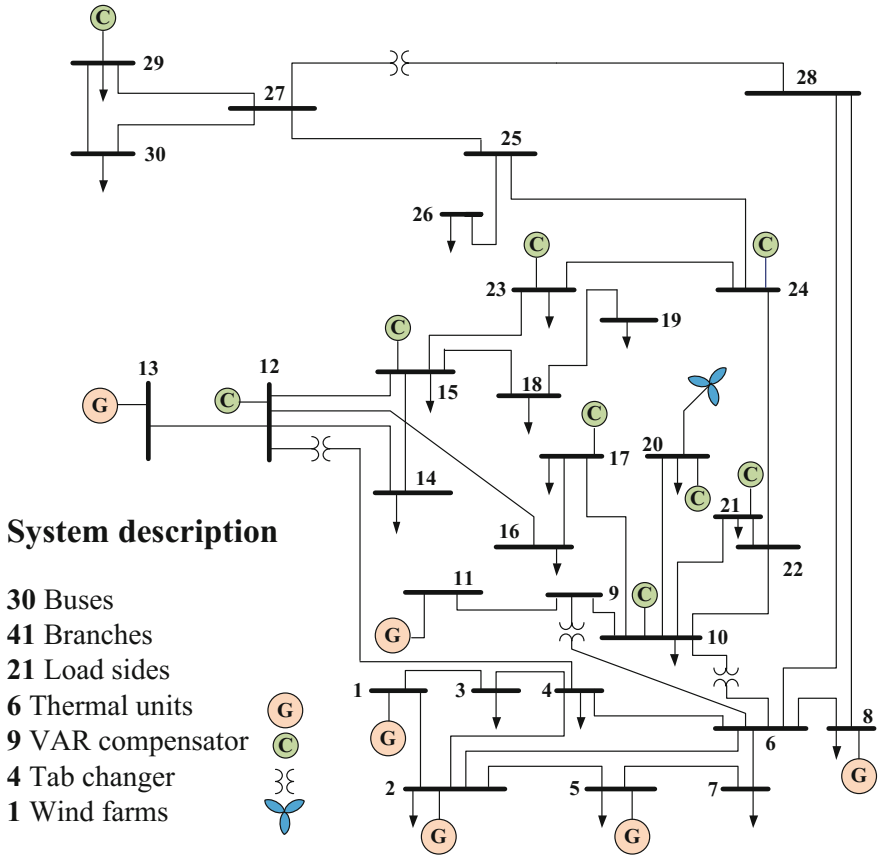

Fig. 12.6 One-line diagram of IEEE 30-bus test system

the remaining 24 buses are *PQ* buses. The network consists of 41 branches, 4 transformers and 9 capacitor banks. Four branches, 6–9, 6–10, 4–12 and 28–27 are under load tap changing transformers. The tap ratios are within the interval [0.9, 1.1]. Additionally, buses 10, 12, 15, 17, 20, 21, 23, 24 and 29 are selected as shunt VAR compensation buses.

In each study we have considered two cases regarding the objective functions. As mentioned in Sect. 12.2, in MO-ORPD problem F_1 with F_2 and F_1 with F_3 are conflicting. Minimization is classified in two part PL/Ξ_{PL} and VD/Ξ_{VD} (Case I) and $PL/$ and LM/Ξ_{LM} (Case II). Figure 12.7 shows the case studies conducted in this chapter. For each case, at first the DMO-ORPD is solved for the sake of comparison with the existing methods, and then SMO-ORPD is solved to investigate the impact of uncertainties on the obtained results.

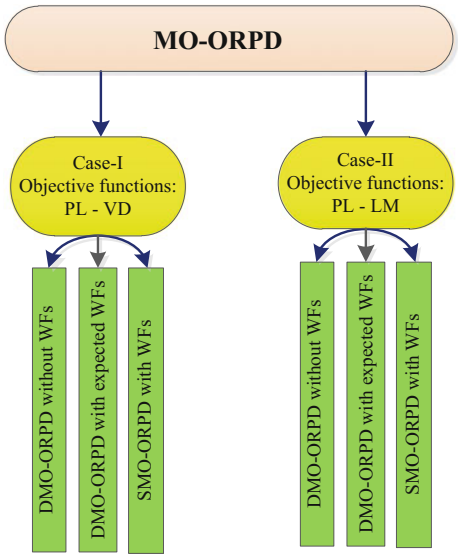

Fig. 12.7 Illustration of the studied cases

12.5.2 Case-I: Active Power Loss Versus Voltage Deviations (PL-VD)

12.5.2.1 Solving DMO-ORPD Without WFs

In this case, the Pareto front is attained for IEEE 30-bus test system without considering any uncertainty and without wind power integration. The VAR compensation devices are modeled by continuous variables for the sake of comparison with the previously published works in literature. The data of compensation limits are available in Appendix (Table 12.15). Table 12.1 summarizes the acquired Pareto solutions for this case. By using min-max fuzzy satisfying criterion, it is observed from Table 12.1 that the best compromise solution is *Solution#16*, with the maximum weakest membership function of 0.7734. The corresponding PL and *VD* are equal to 4.4438 MW and 0.0092, respectively. It is also noticeable that *Solution#1* corresponds to the loss minimization case in *Solution#1,* only *PL* is minimized, and the minimum value of *PL* is obtained 4.2875 MW. The Pareto optimal front of the two objective functions is depicted in Fig. 12.8. For this solution, the optimal values of control variables are given in Table 12.2.

12.5.2.2 Solving DMO-ORPD with Expected WFs

According to Fig. 12.6, IEEE-30 bus is modified and it is presupposed that wind turbine is located in bus 20. In this part, by using Fig. 12.5, the expected value of wind turbine generation is taken account in simulation. Wind power capacity

Table 12.1 Pareto optimal solutions for DMO-ORPD without WFs (Case-I)

#	*PL* (MW)	*VD*	μ_1	μ_2	$\hat{\mu}_r$
1	4.2875	0.0387	1	0	0
2	4.2882	0.0367	0.999	0.0521	0.0521
3	4.2904	0.0348	0.9958	0.1047	0.1047
4	4.2944	0.0328	0.990	0.1574	0.1574
5	4.3005	0.0308	0.9811	0.2101	0.2101
6	4.3092	0.0288	0.9686	0.2627	0.2627
7	4.3190	0.0269	0.9543	0.3154	0.3154
8	4.3293	0.0249	0.9395	0.3681	0.3681
9	4.3401	0.0229	0.9238	0.4207	0.4207
10	4.3515	0.0210	0.9072	0.4734	0.4734
11	4.3637	0.0190	0.8896	0.5260	0.5260
12	4.3767	0.0170	0.8706	0.5787	0.5787
13	4.3909	0.0151	0.8501	0.6314	0.6314
14	4.4064	0.0131	0.8276	0.6840	0.6840
15	4.4238	0.0111	0.8024	0.7367	0.7367
16	4.4438	0.0092	0.7734	0.7894	0.7734
17	4.4680	0.0072	0.7384	0.8420	0.7384
18	4.4999	0.0052	0.6921	0.8947	0.6921
19	4.5544	0.0033	0.6132	0.9473	0.6132
20	4.9774	0.0013	0	1	0

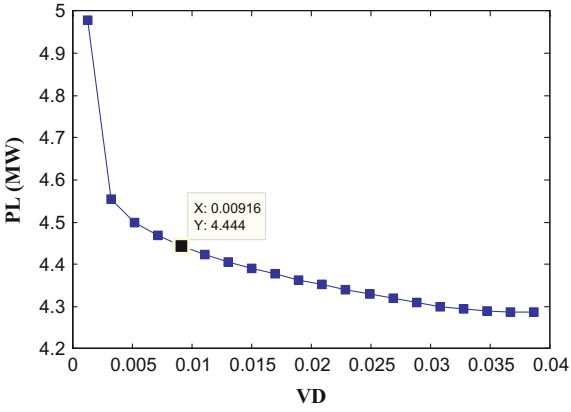

Fig. 12.8 Pareto optimal front for DMO-ORPD without WFs (Case-I)

amounted to twenty percent of the total load on the network is considered. Expected value of wind farm generation is calculated as:

$$P_{w,\exp} = \sum_{s \in \Omega_S} \left(\pi_s \times \zeta_{W_i,s} \times P^r_{W_i} \right) \tag{12.37}$$

Table 12.2 Optimal control variables for the best compromise solution (Solution#16) in (Case-I)

Control parameters	Parameter	DMO-ORPD (without WF)
Generator parameters	V_{g1} (pu)	1.0295
	V_{g2} (pu)	1.0204
	V_{g5} (pu)	1.0093
	V_{g8} (pu)	1.0030
	V_{g11} (pu)	1.0148
	V_{g13} (pu)	1.0258
	P_{g1} (MW)	62.8438
Compensation	Q_{c10} (MVar)	0
	Q_{c12} (MVar)	0
	Q_{c15} (MVar)	3.8495
	Q_{c17} (MVar)	3.6873
	Q_{c20} (MVar)	2.6983
	Q_{c21} (MVar)	6.6481
	Q_{c23} (MVar)	1.7635
	Q_{c24} (MVar)	3.0855
	Q_{c29} (MVar)	2.2464
Transformer tap changer	$t_{6\text{-}9}$	0.9706
	$t_{6\text{-}10}$	1.1000
	$t_{4\text{-}12}$	0.9812
	$t_{28\text{-}27}$	0.9970

It is explained that, discrete steps for compensation devices is used during this section based on the data provided in appendix (Table 12.15). Various Pareto solutions for this part are provided in Table 12.3. In order to solve the multi-objective ORPD problem by ε-constraint method, maximum and minimum values of the real power loss (F_1) and voltage deviation (F_2) are considered, which are equal to 3.8771 MW, 3.1651 MW, 0.0428 pu and 0.0012 pu, respectively. These extreme values are reached by maximizing and minimizing the objective functions of MO-ORPD individually. It means that in *Solution#1* and #20 the objectives are minimizing the *PL* and *VD*, respectively. Among these optimal solutions, *Solution#16* is minimizing both objectives, with the equal to 3.2983 MW PL and the *VD* of 0.0099. Pareto front of answers and control variables for BCS of this case are reported in Fig. 12.9 and Table 12.4, respectively.

12.5.2.3 Solving SMO-ORPD with WFs

In this case the load and wind power uncertainties are considered in the MO-ORPD using the previously described two stage stochastic programming approach.

Table 12.3 Pareto optimal solutions for DMO-ORPD with expected WFs (Case-I)

#	*PL* (MW)	*VD*	μ_1	μ_2	$\hat{\mu}_r$
1	3.1651	0.0428	1	0	0
2	3.166	0.0406	0.9987	0.0526	0.0526
3	3.1696	0.0384	0.9937	0.1052	0.1052
4	3.1759	0.0362	0.9849	0.1579	0.1579
5	3.183	0.0340	0.9749	0.2105	0.2105
6	3.1904	0.0318	0.9645	0.2631	0.2631
7	3.1982	0.0296	0.9535	0.3158	0.3158
8	3.2064	0.0275	0.9421	0.3684	0.3684
9	3.215	0.0253	0.9300	0.4210	0.4210
10	3.2241	0.0231	0.9172	0.4737	0.4737
11	3.234	0.0209	0.9032	0.5263	0.5263
12	3.2445	0.0187	0.8886	0.5789	0.5789
13	3.2556	0.0165	0.8729	0.6316	0.6316
14	3.2681	0.0143	0.8553	0.6842	0.6842
15	3.2823	0.0121	0.8355	0.7368	0.7368
16	3.2983	0.0099	0.8129	0.7895	0.7895
17	3.3182	0.0077	0.7850	0.8421	0.7850
18	3.3453	0.0055	0.7470	0.8947	0.7470
19	3.3928	0.0033	0.6801	0.9474	0.6801
20	3.8771	0.0012	0	1	0

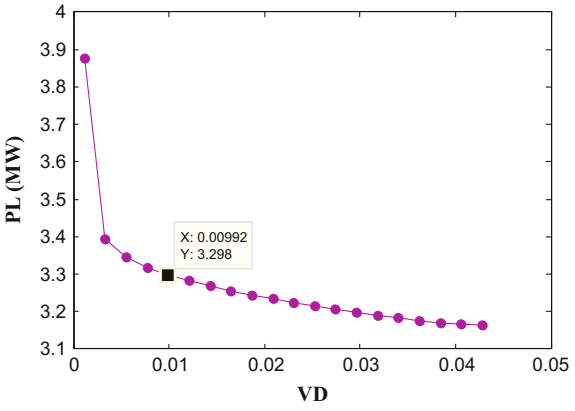

Fig. 12.9 Pareto front of DMO-ORPD with WFs (Case-I)

The attained Pareto optimal solutions in this case are presented in Table 12.5. It is observed from this table that Ξ_{PL} varies from 3.4003 to 4.1891 MW, while Ξ_{VD} varies from 0.0431 to 0.0013, respectively. The *Solution#1* corresponds to the Ξ_{PL} minimization case, where the minimum value of 3.4003 MW is obtained for Ξ_{PL},

Table 12.4 Optimal control variables for the best compromise solution (Solution#16) in DMO-ORPD with expected wind-(Case-I)

Control parameters	Parameter	DMO-ORPD (with WF)
Generator parameters	V_{g1} (pu)	1.0236
	V_{g2} (pu)	1.0161
	V_{g5} (pu)	1.0062
	V_{g8} (pu)	1.0015
	V_{g11} (pu)	1.0156
	V_{g13} (pu)	1.0248
	P_{g1} (MW)	48.2003
Compensation (switching steps)	u_{c10}	0
	u_{c12}	0
	u_{c15}	1
	u_{c17}	2
	u_{c20}	1
	u_{c21}	3
	u_{c23}	1
	u_{c24}	3
	u_{c29}	1
Wind farms parameters	P_{w19} (MW)	29.222
	Q_{w19} (MVar)	2.2632
Transformer tap changer	$t_{6\text{-}9}$	0.9711
	$t_{6\text{-}10}$	1.1000
	$t_{4\text{-}12}$	0.9840
	$t_{28\text{-}27}$	0.9936

whereas *Solution#20* deals with the case of Ξ_{VD} minimization, in which the minimum value of Ξ_{VD} is 0.0431. It is observed from Table 12.5 that *Solution#16* is the best compromise solution, with Ξ_{PL} equals to 3.5475 MW and Ξ_{VD} equals to 0.0101. Also, Fig. 12.10 depicts the obtained optimal Pareto front in this case.

Table 12.6 summarizes the obtained optimal *here and now* control variables for the best compromise solution. Also, the optimal values of *wait and see* control variables are depicted in Figs. 12.11, 12.12 and 12.13, in all possible scenarios. Figure 12.11 shows the active power generation at the slack bus (bus 1) in all 15 scenarios. Figure 12.12 represents the active/reactive power output of the wind farm in all scenarios. The optimal amount of reactive power compensation steps are also given in Fig. 12.13.

Table 12.5 Pareto optimal solutions for SMO-ORPD (Case-I)

#	Ξ_{PL} (MW)	Ξ_{LM}	μ_1	μ_2	$\hat{\mu}_r$
1	3.4003	0.0431	1	0	0
2	3.4188	0.0409	0.9765	0.0526	0.0526
3	3.4194	0.0387	0.9758	0.1053	0.1053
4	3.4213	0.0365	0.9734	0.1579	0.1579
5	3.4253	0.0343	0.9683	0.2105	0.2105
6	3.4322	0.0321	0.9595	0.2632	0.2632
7	3.4405	0.0299	0.9490	0.3158	0.3158
8	3.4492	0.0277	0.9380	0.3684	0.3684
9	3.4584	0.0255	0.9264	0.4211	0.4211
10	3.4681	0.0233	0.914	0.4737	0.4737
11	3.4785	0.0211	0.9008	0.5263	0.5263
12	3.4897	0.0189	0.8867	0.5790	0.5790
13	3.5018	0.0167	0.8713	0.6316	0.6316
14	3.5152	0.0145	0.8543	0.6842	0.6842
15	3.5302	0.0123	0.8353	0.7368	0.7368
16	3.5475	0.0101	0.8133	0.7895	0.7895
17	3.5687	0.0079	0.7865	0.8421	0.7865
18	3.5949	0.0057	0.7533	0.8947	0.7533
19	3.6396	0.0035	0.6967	0.9474	0.6967
20	4.1891	0.0013	0	1	0

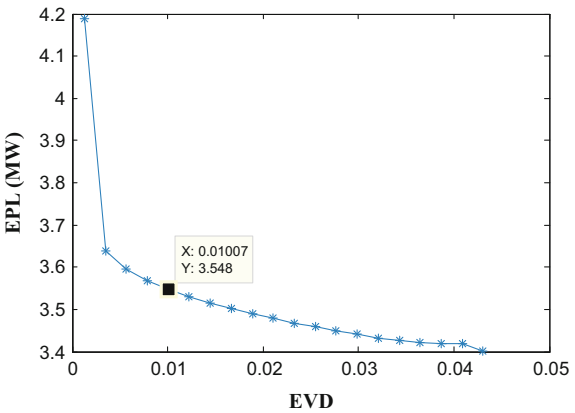

Fig. 12.10 Pareto front of SMO-ORPD (Case-I)

Table 12.6 Optimal values for here and now control variables at the best compromise solution (Solution#16) in Case-I

Control parameters	Parameter	DMO-ORPD(without WF)
Generator parameters	V_{g1} (pu)	1.0270
	V_{g2} (pu)	1.0193
	V_{g5} (pu)	1.0089
	V_{g8} (pu)	1.0043
	V_{g11} (pu)	1.0165
	V_{g13} (pu)	1.0267
Transformer tap changer	$t_{6\text{-}9}$	0.9694
	$t_{6\text{-}10}$	1.1000
	$t_{4\text{-}12}$	0.9841
	$t_{28\text{-}27}$	0.9933

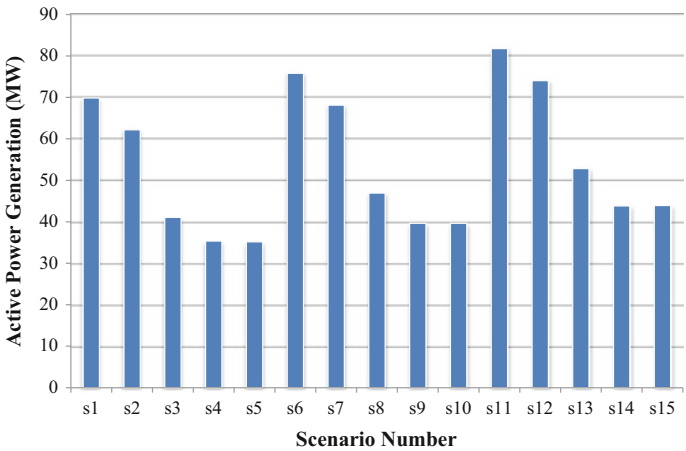

Fig. 12.11 Active power generation in slack bus (bus 1) in all scenarios (in MW)-(Case-I)

12.5.3 Case-II: Active Power Loss Versus L_{max}, *(PL-LM)*

12.5.3.1 Solving DMO-ORPD Without WFs

In this case, *PL* and *LM* are considered as the two considered conflicted objectives. The Pareto front is obtained without considering any uncertainty. Table 12.7 summarizes the obtained Pareto solutions for this case. By using min-max fuzzy

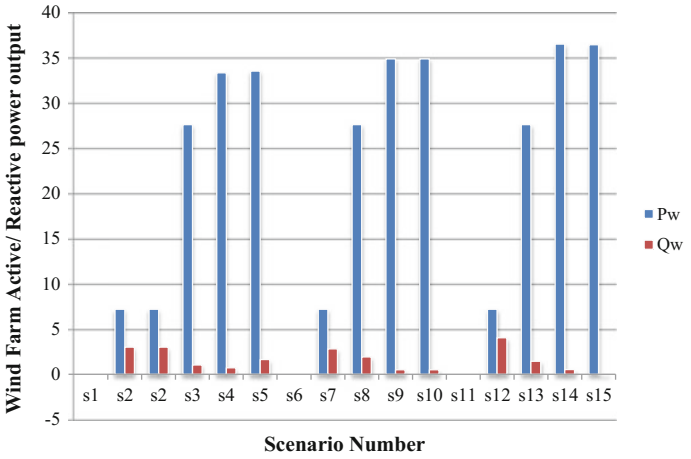

Fig. 12.12 Active/reactive power output of wind farm (located at bus 20) in all scenarios (in MW and MVAR) - (Case-I)

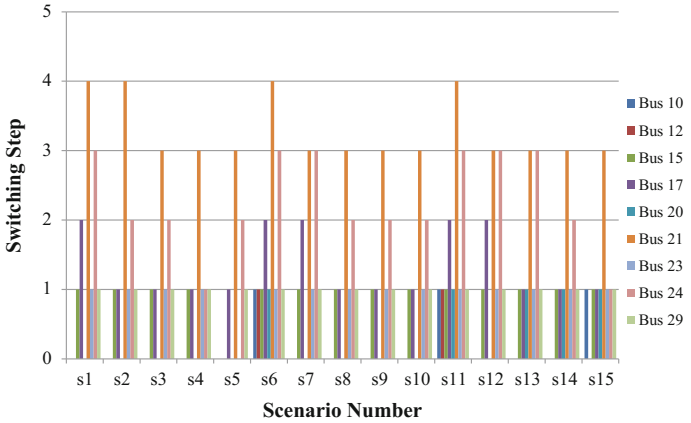

Fig. 12.13 Switching steps in VAR compensation buses at different scenarios (Case-I)

satisfying method, it is evident from Table 12.7 that the best compromise solution is *Solution#17*, with the maximum weakest membership function of 0.7988. The corresponding PL and *LM* are equal to 4.6106 MW and 0.1199 pu, respectively. Pareto front of this case is available in Fig. 12.14. Table 12.8 summarizes the obtained control variables for the best compromise solution, *Solution#17*, of this case.

Table 12.7 Pareto optimal solutions for DMO-ORPD without WFs (Case-II)

#	*PL* (MW)	*LM*	μ_1	μ_2	$\hat{\mu}_r$
1	4.2875	0.1323	1	0	0
2	4.2879	0.1315	0.9997	0.0526	0.0526
3	4.2893	0.1308	0.9989	0.1053	0.1053
4	4.2918	0.1300	0.9973	0.1579	0.1579
5	4.2956	0.1292	0.9949	0.2105	0.2105
6	4.3012	0.1284	0.9915	0.2632	0.2632
7	4.3087	0.1277	0.9868	0.3158	0.3158
8	4.3187	0.1269	0.9806	0.3684	0.3684
9	4.3318	0.1261	0.9724	0.4210	0.4210
10	4.3475	0.1253	0.9626	0.4737	0.4737
11	4.3659	0.1246	0.9512	0.5263	0.5263
12	4.3869	0.1238	0.9381	0.5789	0.5789
13	4.4105	0.1230	0.9234	0.6316	0.6316
14	4.4403	0.1222	0.9048	0.6842	0.6842
15	4.4835	0.1215	0.8779	0.7368	0.7368
16	4.5413	0.1207	0.8420	0.7895	0.7895
17	4.6106	0.1199	0.7988	0.8421	0.7988
18	4.7219	0.1191	0.7295	0.8947	0.7295
19	5.0212	0.1184	0.5431	0.9474	0.5431
20	5.8934	0.1176	0	1	0

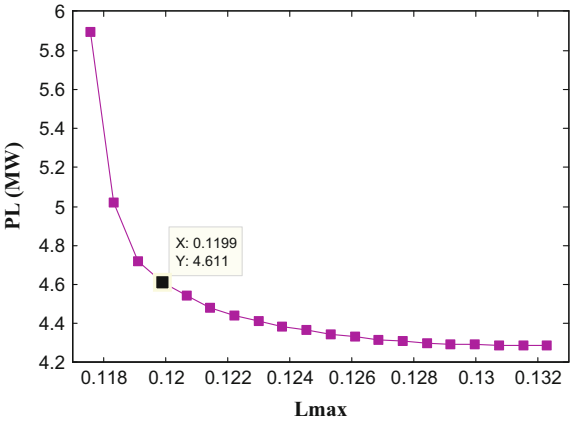

Fig. 12.14 Pareto front of DMO-ORPD without WFs (Case-II)

12.5.3.2 Solving DMO-ORPD with Expected WFs

Similar to Case-I, in this case, expected value of wind power as an input power is calculated by Eq. 12.37. Table 12.9 shows the obtained 20 selected Pareto solutions for this case. Among this answers, *Solution#17* has minimized both objective simultaneously with $PL = 3.2751$ and $LM = 0.1146$. Figure 12.15 depicts the

Table 12.8 Optimal control variables for the best compromise solution (Solution#17) in DMO-ORPD without wind-Case-II

Control parameters	Parameter	DMO-ORPD (without WF)
Generator parameters	V_{g1} (pu)	1.0366
	V_{g2} (pu)	1.0286
	V_{g5} (pu)	1.0182
	V_{g8} (pu)	1.0134
	V_{g11} (pu)	1.0110
	V_{g13} (pu)	1.0434
	P_{g1} (MW)	63.0106
Compensation	Q_{c10} (MVar)	8.2754
	Q_{c12} (MVar)	0
	Q_{c15} (MVar)	0
	Q_{c17} (MVar)	7.0185
	Q_{c20} (MVar)	4.0128
	Q_{c21} (MVar)	14.2677
	Q_{c23} (MVar)	2.9065
	Q_{c24} (MVar)	7.7563
	Q_{c29} (MVar)	0
Transformer tap changer	$t_{6\text{-}9}$	1.0706
	$t_{6\text{-}10}$	0.9000
	$t_{4\text{-}12}$	0.9956
	$t_{28\text{-}27}$	0.9719

Pareto front of this case. According to Fig. 12.15, it is clear that when wind power injected into the network, it substantially reduces network losses and increases network stability. Table 12.10 presents the obtained control variables for best solution of this case (*Solution#17*).

12.5.3.3 Solving SMO-ORPD with WFs

The uncertainty is modeled using scenario based approach for Case-II and results of Pareto solutions are presented in Table 12.11. Figure 12.16 shows the Pareto front for Case-II with considering load and wind uncertainties using scenario based approach.

Similar to Case-I, *here and now* control variables are shown in Table 12.12 and *wait and see* control variables are shown in Figs. 12.17, 12.18 and 12.19. It should be noticed that, these variables are presented for BCS (*Solution#16*).

Table 12.9 Pareto optimal solutions for DMO-ORPD with expected WFs (Case-II)

#	*PL* (MW)	*LM*	μ_1	μ_2	$\hat{\mu}_r$
1	3.1651	0.1247	1	0	0
2	3.1654	0.1241	0.9994	0.0526	0.0526
3	3.1662	0.1234	0.9979	0.1053	0.1053
4	3.1682	0.1228	0.9943	0.1579	0.1579
5	3.1707	0.1222	0.9895	0.2105	0.2105
6	3.1742	0.1215	0.9832	0.2632	0.2632
7	3.1786	0.1209	0.9749	0.3158	0.3158
8	3.1841	0.1203	0.9647	0.3684	0.3684
9	3.1905	0.1196	0.9528	0.4210	0.4210
10	3.1977	0.1190	0.9395	0.4737	0.4737
11	3.2056	0.1184	0.9247	0.5263	0.5263
12	3.2144	0.1178	0.9084	0.5789	0.5789
13	3.2242	0.1171	0.8901	0.6316	0.6316
14	3.235	0.1165	0.8700	0.6842	0.6842
15	3.2468	0.1159	0.8481	0.7368	0.7368
16	3.2597	0.1152	0.8241	0.7895	0.7895
17	3.2751	0.1146	0.7955	0.8421	0.7955
18	3.2944	0.1140	0.7594	0.8947	0.7594
19	3.3189	0.1133	0.7139	0.9473	0.7139
20	3.7027	0.1127	0	1	0

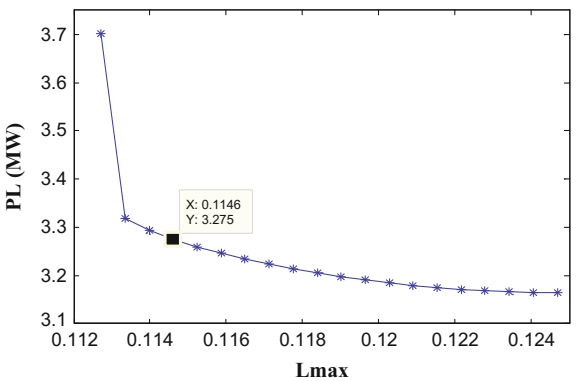

Fig. 12.15 Pareto front of DMO-ORPD with WFs (Case-II)

Table 12.10 Optimal control variables for the best compromise solution (Solution#17) in Case-II

Control parameters	Parameter	DMO-ORPD (with WF)
Generator parameters	V_{g1} (pu)	1.0371
	V_{g2} (pu)	1.0301
	V_{g5} (pu)	1.0204
	V_{g8} (pu)	1.0161
	V_{g11} (pu)	1.0136
	V_{g13} (pu)	1.0461
	P_{g1} (MW)	49.3914
Compensation (switching steps)	u_{c10}	0
	u_{c12}	0
	u_{c15}	1
	u_{c17}	2
	u_{c20}	1
	u_{c21}	4
	u_{c23}	1
	u_{c24}	3
	u_{c29}	1
Wind Farms parameters	P_{w20} (MW)	29.2220
	Q_{w20} (MVar)	2.4846
Transformer tap changer	$t_{6\text{-}9}$	1.0550
	$t_{6\text{-}10}$	0.9000
	$t_{4\text{-}12}$	0.9930
	$t_{28\text{-}27}$	0.9761

12.6 Discussions on the Results

12.6.1 Comparison of DMO-ORPD Performance with Pervious Literature

In Tables 12.13 and 12.14 the obtained *PL*, *VD* and *LM* are compared with the results reported by some recently published algorithms. Table 12.13 shows the obtained *PL* and *VD* for *Solution#1* (*PL* minimization), *Solution#20* (*VD* minimization), and *Solution#16* (compromise solution), whereas Table 12.14 give a comparison for *PL* and *LM*. *Solution#1* (*PL* minimization), *Solution#20* (*LM* minimization), and *Solution#17* (compromise solution) are compared with recently published works. According to these tables, it can be observed that the obtained

Table 12.11 Pareto optimal solutions for SMO-ORPD) (Case-II)

#	Ξ_{PL} (MW)	Ξ_{LM}	μ_1	μ_2	$\hat{\mu}_r$
1	3.4815	0.1258	1	0	0
2	3.4865	0.1251	0.9915	0.0635	0.0635
3	3.4881	0.1245	0.9887	0.1264	0.1264
4	3.4914	0.1239	0.9831	0.1890	0.1890
5	3.4918	0.1233	0.9824	0.2513	0.2513
6	3.4942	0.1227	0.9783	0.3131	0.3131
7	3.4989	0.1221	0.9702	0.3745	0.3745
8	3.5048	0.1215	0.9601	0.4352	0.4352
9	3.5118	0.1209	0.9481	0.4952	0.4952
10	3.5196	0.1204	0.9347	0.5541	0.5541
11	3.5279	0.1198	0.9204	0.6117	0.6117
12	3.5375	0.1193	0.9040	0.6675	0.6675
13	3.5485	0.1188	0.8851	0.7208	0.7208
14	3.5602	0.1183	0.8650	0.7703	0.7703
15	3.573	0.1179	0.8431	0.8143	0.8143
16	3.5873	0.1175	0.8187	0.8488	0.8187
17	3.6039	0.1174	0.7901	0.8658	0.7901
18	3.6214	0.1172	0.7600	0.8863	0.7600
19	3.6399	0.1171	0.7283	0.8942	0.7283
20	4.0646	0.1161	0	1	0

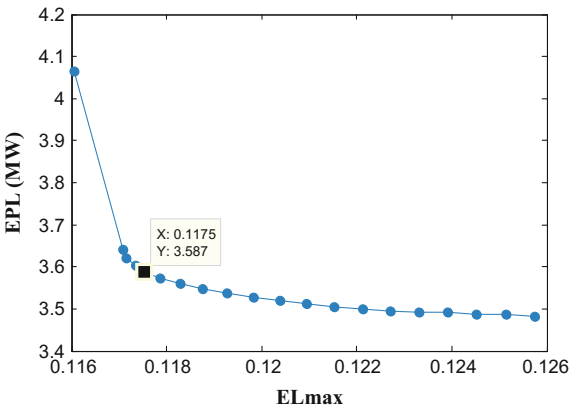

Fig. 12.16 Pareto front of SMO-ORPD (Case-II)

Table 12.12 Optimal values for here and now control variables at the best compromise solution (Solution#16) in Case-II

Control parameters	Parameter	DMO-ORPD (without WF)
Generator parameters	V_{g1} (pu)	1.0151
	V_{g2} (pu)	0.9976
	Vg_5 (pu)	1.0083
	V_{g8} (pu)	1.0092
	V_{g11} (pu)	1.0246
	V_{g13} (pu)	1.0398
Transformer tap changer	$t_{6\text{-}9}$	1.0455
	$t_{6\text{-}10}$	0.9000
	$t_{4\text{-}12}$	0.9821
	$t_{28\text{-}27}$	0.9698

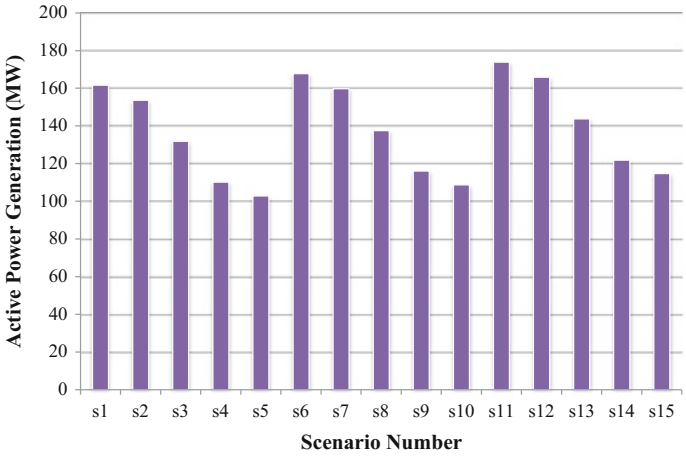

Fig. 12.17 Active power generation in slack bus (bus 1) in all scenarios (in MW)-(Case-II)

solutions are superior to the previously reported ones like as gravitational search algorithm (GSA) [17], differential evolutionary algorithm [15], quasi-oppositional teaching learning based optimization (TLBO) algorithm [25] and chaotic parallel vector evaluated interactive honey bee mating optimization (CPVEIHBMO) [26].

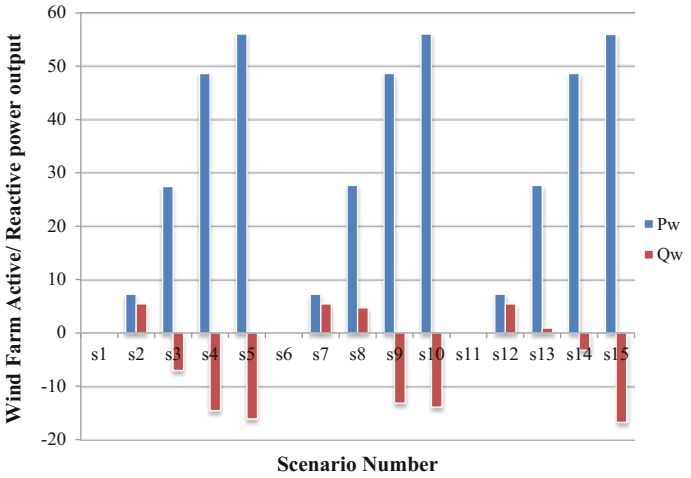

Fig. 12.18 Active and reactive power output of wind farm (located at bus 20) in all scenarios (in MW and MVAR)—(Case-II)

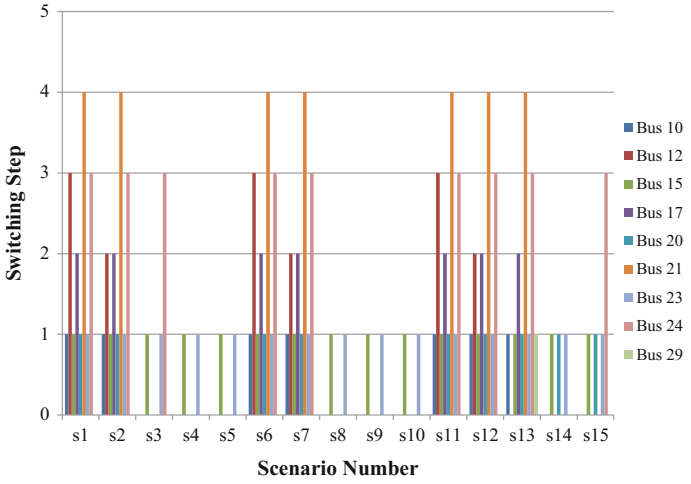

Fig. 12.19 Switching steps in VAR compensation buses at different scenarios (Case-II)

Table 12.13 Comparison of the obtained *PL* and *VD* in DMO-ORPD (without WFs), with the published methods

	PL Minimization	*VD* Minimization	*PL* (MW) Compromise solution
Proposed	4.2875	4.9774	4.4438
CPVEIHBMO [26]	4.37831	4.994831	5.3243
HBMO [26]	4.40867	5.2092	5.535
QOTLBO [25]	4.5594	6.4962	5.2594
NSGA-II [27]	5.137	5.686	–
DE [15]	4.555	6.4755	–
SPMGSO [27]	5.123	5.96	–
GSA [17]	4.5143	4.9752	–
	PL minimization	*VD* minimization	*VD* (pu) Compromise solution
Proposed	0.0387	0.0013	0.0092
CPVEIHBMO [26]	0.67352	0.198756	0.7397
HBMO [26]	0.87364	0.2106	0.87664
QOTLBO [25]	1.9057	0.0856	0.121
NSGA-II [27]	0.6443	0.1789	–
DE [15]	1.9989	0.0911	–
SPMGSO [27]	0.73986	0.1438	–
GSA [17]	0.8752	0.2157	–

12.6.2 Impact of Wind Energy on MO-ORPD Problem

Figures 12.20 and 12.21 summarize the obtained results of DMO-ORPD with and without WFs and SMO-ORPD for both Case-I and Case-II. According to Fig. 12.20a, it is clear that by installing wind farms on the system, real power losses (*PL* in deterministic and *EPL* in stochastic model) are reduced considerably. It is also observed from this figure that in the case of SMO-ORPD, the *EPL* is higher than the case of DMO-ORPD with expected wind. Besides, Fig. 12.20b depicts the obtained values for *VD* and *EVD* in both Case-I and II. It is evidently observed from this figure that, installation of wind farm leads to deterioration of voltage deviations, especially in the case of SMO-OPRD. This is mainly because of fluctuations of wind farm output power, in different scenarios.

Also, Fig. 12.21 shows the obtained values of *PL* (and *EPL*) along with $L_{\max}$ (and ELM) in Case-II. According to Fig. 12.21a active power losses are decreased when the wind farm is considered, both in DMO-ORPD (with wind farm) and SMO-ORPD. Besides, according to Fig. 12.21b the voltage stability of system increases in the presence of wind farm, since the $L_{\max}$ and *ELM* reduced in both DMO-ORPD (with wind farm) and SMO-ORPD cases.

Table 12.14 Comparison of the obtained PL and LM in DMO-ORPD (without WFs), with the published methods

	PL minimization	*LM* minimization	*PL* (MW) Compromise solution
Proposed	4.2875	5.8934	4.6106
CPVEIHBMO [26]	4.7831	6.6501	5.3243
HBMO [26]	4.40867	6.66	5.5352
QOTLBO [25]	4.5594	5.2554	5.2594
MOCIPSO [24]	5.174	5.419	5.232
MOPSO [24]	5.233	5.528	5.308
DE [15]	4.555	7.0733	–
RGA [22]	4.951	5.0912	–
CMAES [22]	4.945	5.129	–
GSA [17]	4.5143	6.6602	–
	PL minimization	*LM* minimization	*LM* (pu) Compromise solution
Proposed	0.1323	0.1176	0.1199
CPVEIHBMO [26]	0.141	0.116	-
HBMO [26]	0.12101	0.111	0.1163
QOTLBO [25]	0.1263	0.1147	0.1203
MOCIPSO [24]	0.1273	0.1242	0.1254
MOPSO [24]	0.12664	0.1141	11.821
DE [15]	0.1317	0.1192	0.12191
RGA [22]	0.5513	0.1246	–
CMAES [22]	0.13965	0.1386	–
GSA [17]	0.13944	0.1382	–

The obtained results imply the positive impact of wind power generation on the voltage stability enhancement and decreasing system real power losses. Also, it can be observed that the installed wind farm has little effects on the voltage deviations.

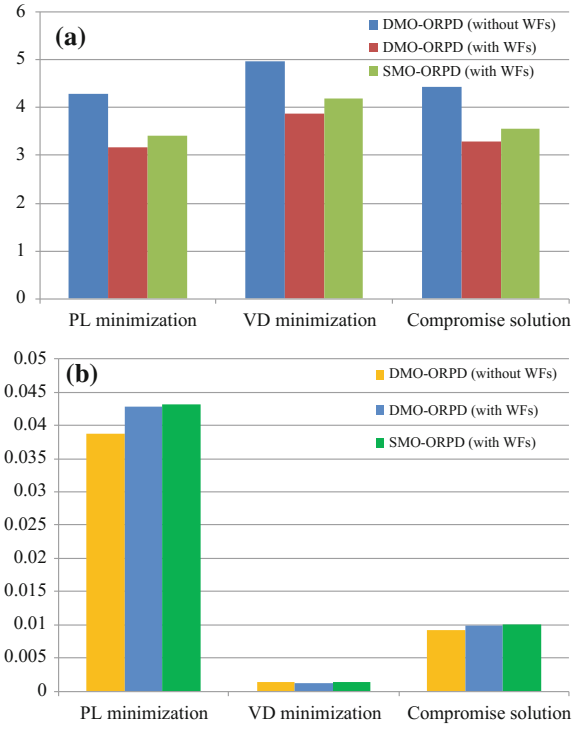

Fig. 12.20 Comparison of the obtained results of Case-I in different conditions, **a** *PL* and *EPL* (MW), **b** *VD* and *EVD* (pu)

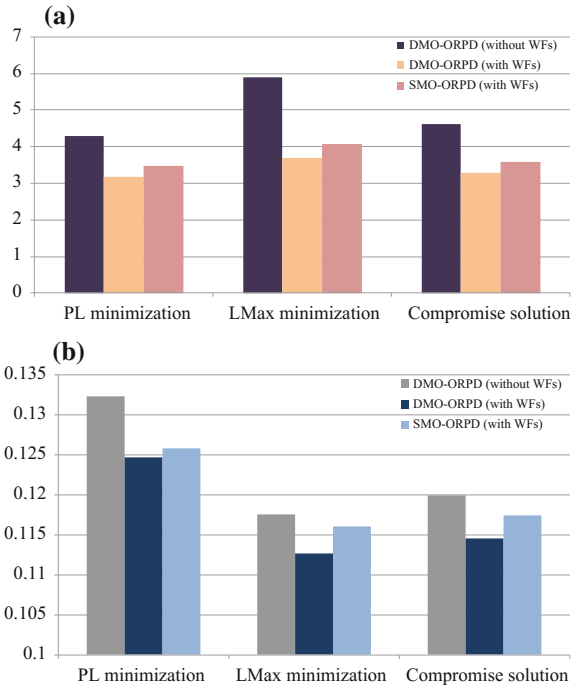

Fig. 12.21 Comparison of the obtained results of Case-II in different conditions, **a** *PL* and *EPL* (MW), **b** *LM* and EL_{max}

12.7 Conclusions

In this chapter the stochastic multi-objective optimal reactive power dispatch (SMO-ORPD) problem in a wind integrated power system is studied by considering the uncertainties of system load and wind power generations. For decision making under the above uncertainties two-stage stochastic optimization model is utilized. In the multi-objective optimization framework real power losses, voltage deviation and voltage stability improvement index (*L*-index) are optimized simultaneously. The ε-constraint method is utilized to solve multi-objective optimization problem. The obtained results in the deterministic case are compared with the recently applied intelligent search-based algorithms and it is found that the suggested method can find better solutions for both objective functions in this case.

In the stochastic case, a comprehensive set of decision variables including *here and now* and *wait and see* control variables are obtained. The offered SMO-ORPD model is verified using the IEEE 30-bus test system. The numerical results substantiate that in the presence of wind power generation, the expected value of active power losses and *L*-index are reduced in comparison with the deterministic case. This confirms the positive influence of wind power generation on the reduction of system losses.

Appendix

See Table 12.15.

Table 12.15 The data of VAR Compensation devices

Bus No.	DMO-ORPD without WFs [26, 47]		DMO-ORPDwith WFs SMO-ORPD with WFs		
	$Q_{C_i}^{\min}$ (MVAR)	$Q_{C_i}^{\max}$(MVAR)	$I_{C_i}^{\min}$	$I_{C_i}^{\max}$	Q_{C_i} (MVAR)
10	0	36	0	1	1
12	0	36	0	3	1.5
15	0	36	0	1	1.5
17	0	36	0	2	2
20	0	36	0	1	0.5
21	0	36	0	4	2
23	0	36	0	1	1
24	0	36	0	3	1.5
29	0	36	0	1	0.5

References

1. B. Zhao, C. Guo, Y. Cao, A Multiagent-Based Particle Swarm Optimization Approach for Optimal Reactive Power Dispatch, IEEE Transactions on Power Systems, vol. 20, pp. 1070–1078, 2005.
2. C. Dai, W. Chen, Y. Zhu, X. Zhang, Seeker Optimization Algorithm for Optimal Reactive Power Dispatch, IEEE Transactions on Power Systems, vol. 24, pp. 1218–1231, 2009.
3. A. Khorsandi, A. Alimardani, B. Vahidi, S. Hosseinian, Hybrid Shuffled Frog Leaping Algorithm and Nelder-Mead Simplex Search for Optimal Reactive Power Dispatch, IET Generation, Transmission & Distribution, vol. 5, pp. 249–256, 2011.
4. M. Ghasemi, S. Ghavidel, M.M. Ghanbarian, A. Habibi, A New Hybrid Algorithm for Optimal Reactive Power Dispatch Problem with Discrete and Continuous Control Variables, Applied Soft Computing vol. 22, pp. 126–40, 2014.
5. M. Ghasemi, M.M. Ghanbarian, S. Ghavidel, S. Rahmani, E. Mahboubi Moghaddam, Modified Teaching Learning Algorithm and Double Differential Evolution Algorithm for Optimal Reactive Power Dispatch Problem: A Comparative Study, Information Sciences, vol. 278, pp. 231–249, 2014.
6. M. Martinez Rojas, A. Sumper, O. Gomis Bellmunt, A. Sudria Andreu, Reactive Power Dispatch in Wind Farms Using Particle Swarm Optimization Technique and Feasible Solutions Search, Applied Energy, vol. 88, pp. 4678–4686, 2011.
7. R. Mallipeddi, S. Jeyadevi, P.N. Suganthan, S. Baskar, Efficient Constraint Handling for Optimal Reactive Power Dispatch Problems, Swarm and Evolutionary Computation, vol. 5, pp. 28–36, 2012.
8. C.M. Huang, S.J. Chen, Y.C. Huang, H.T. Yang, Comparative Study of Evolutionary Computation Methods for Active-Reactive Power Dispatch, IET Generation, Transmission & Distribution, vol. 6, pp. 636–645, 2012.
9. A. Rajan, T. Malakar, Optimal Reactive Power Dispatch Using Hybrid Nelder-Mead Simplex Based Firefly Algorithm, International Journal of Electrical Power & Energy Systems, vol. 66, pp. 9–24, 2015.
10. R.P. Singh, V. Mukherjee, S. Ghoshal, Optimal Reactive Power Dispatch by Particle Swarm Optimization with an Aging Leader and Challengers, Applied Soft Computing, vol. 29, pp. 298–309, 2015.
11. M.H. Sulaiman, Z. Mustaffa, M.R. Mohamed, O. Aliman, Using the Gray Wolf Optimizer for Solving Optimal Reactive Power Dispatch Problem, Applied Soft Computing, vol. 32, pp. 286–292, 2015.
12. D. Thukaram, G. Yesuratnam, Optimal Reactive Power Dispatch in a Large Power System with AC-DC and FACTS Controllers, Generation, Transmission & Distribution, IET, vol. 2, pp. 71–81, 2008.
13. A. Rabiee, M. Vanouni, M. Parniani, Optimal Reactive Power Dispatch for Improving Voltage Stability Margin Using a Local Voltage Stability Index, Energy Conversion and Management, vol. 59, pp. 66–73, 2012.
14. C. Dai, W. Chen, Y. Zhu, and X. Zhang, Reactive Power Dispatch Considering Voltage Stability with Seeker Optimization Algorithm, Electric Power Systems Research, vol. 79, pp. 1462–1471, 2009.
15. A. Ela, M. Abido, S. Spea, Differential Evolution Algorithm for Optimal Reactive Power Dispatch, Electric Power Systems Research, vol. 81, pp. 458–464, 2011.
16. A. Khazali, M. Kalantar, Optimal Reactive Power Dispatch Based on Harmony Search Algorithm, International Journal of Electrical Power & Energy Systems, vol. 33, pp. 684–692, 2011.
17. S. Duman, Y. Sonmez, U. Guvenc, N. Yorukeren, Optimal Reactive Power Dispatch Using a Gravitational Search Algorithm, IET Generation, Transmission & Distribution, vol. 6, pp. 563–576, 2012.

18. J.M. Ramirez, J.M. Gonzalez, T.O. Ruben, An Investigation about the Impact of the Optimal Reactive Power Dispatch Solved by DE, International Journal of Electrical Power & Energy Systems, vol. 33, pp. 236–244, 2011.
19. E.M. Soler, E.N. Asada, G.R. Da Costa, Penalty-Based Nonlinear Solver for Optimal Reactive Power Dispatch with Discrete Controls, IEEE Transactions on Power Systems, vol. 28, pp. 2174–2182, 2013.
20. M. Abido, J. Bakhashwain, Optimal VAR Dispatch Using a Multi-Objective Evolutionary Algorithm, International Journal of Electrical Power & Energy Systems, vol. 27, pp. 13–20, 2005.
21. L. Zhihuan, L. Yinhong, D. Xianzhong, Non-Dominated Sorting Genetic Algorithm-II for Robust Multi-Objective Optimal Reactive Power Dispatch, Generation, Transmission & Distribution, IET, vol. 4, pp. 1000–1008, 2010.
22. S. Jeyadevi, S. Baskar, C. Babulal, M. Willjuice Iruthayarajan, Solving Multi-Objective Optimal Reactive Power Dispatch Using Modified NSGA-II, International Journal of Electrical Power & Energy Systems, vol. 33, pp. 219–228, 2011.
23. A. Saraswat, A. Saini, Multi-Objective Optimal Reactive Power Dispatch Considering Voltage Stability in Power Systems Using HFMOEA, Engineering Applications of Artificial Intelligence, vol. 26, pp. 390–404, 2013.
24. G. Chen, L. Liu, P. Song, Y. Du, Chaotic Improved PSO-Based Multi-Objective Optimization for Minimization of Power Losses and L Index in Power Systems, Energy Conversion and Management, vol. 86, pp. 548–560, 2014.
25. B. Mandal, P.K. Roy, Optimal Reactive Power Dispatch Using Quasi-Oppositional Teaching Learning Based Optimization, International Journal of Electrical Power & Energy Systems, vol. 53, pp. 123–134, 2013.
26. A. Ghasemi, K. Valipour, A. Tohidi, Multi-Objective Optimal Reactive Power Dispatch Using a New Multi-Objective Strategy, International Journal of Electrical Power & Energy Systems, vol. 57, pp. 318–334, 2014.
27. B. Zhou, K. Chan, T. Yu, H. Wei, J. Tang, Strength Pareto Multi-Group Search Optimizer for Multi-Objective Optimal VAR Dispatch, IEEE Transactions on Industrial Informatics, vol. 10, pp. 1012–1022, 2014.
28. Z. Hu, X. Wang, G. Taylor, Stochastic Optimal Reactive Power Dispatch: Formulation and Solution Method, International Journal of Electrical Power & Energy Systems, vol. 32, pp. 615–621, 2010.
29. S. M. Mohseni Bonab, A. Rabiee, S. Jalilzadeh, B. Mohammadi Ivatloo, and S. Nojavan, "Probabilistic Multi Objective Optimal Reactive Power Dispatch Considering Load Uncertainties Using Monte Carlo Simulations, Journal of Operation and Automation in Power Engineering, vol. 3(1), pp. 83–93, 2015.
30. S. M. Mohseni Bonab, A. Rabiee, B. Mohammadi Ivatloo, Load Uncertainty Analysis in Multi Objective Optimal Reactive Power Dispatch Considering Voltage Stability, Majlesi Journal of Energy Management, vol. 4(2), pp. 23–30, 2015.
31. A. Brooke, D. Kendrick, A. Meeraus, GAMS Release 2.25: A User's Guide: GAMS Development Corporation Washington, DC, 1996.
32. P.E. Gill, W. Murray, M.A. Saunders, SNOPT: An SQP Algorithm for Large-Scale Constrained Optimization, SIAM Journal on Optimization, vol. 12, pp. 979–1006, 2002.
33. The GAMS Software Website, http://www.gams.com/dd/docs/solvers/sbb.pdf, 2013.
34. A. Soroudi, T. Amraee, Decision Making under Uncertainty in Energy Systems: State of the Art, Renewable and Sustainable Energy Reviews, vol. 28, pp. 376–384, 2013.
35. A. Rabiee, A. Soroudi, B. Mohammadi Ivatloo, M. Parniani, Corrective Voltage Control Scheme Considering Demand Response and Stochastic Wind Power, IEEE Transactions on Power Systems, vol. 29, pp. 2965–2973, 2014.
36. A. Soroudi, B. Mohammadi Ivatloo, A. Rabiee, Energy Hub Management with Intermittent Wind Power, in Large Scale Renewable Power Generation, Springer, pp. 413–438, 2014.

37. A. Rabiee, A. Soroudi, Stochastic Multiperiod OPF Model of Power Systems with HVDC-Connected Intermittent Wind Power Generation, IEEE Transactions on Power Delivery, vol. 29, pp. 336–344, 2014.
38. A. Soroudi, A. Rabiee, A. Keane, Stochastic Real-Time Scheduling of Wind-Thermal Generation Units in an Electric Utility, IEEE System Journal, 2014.
39. R.D. Zimmerman, C.E. Murillo Sanchez, D. Gan, A MATLAB Power System Simulation Package, 2005.
40. S. Wen, H. Lan, Q. Fu, D. Yu, L. Zhang, Economic Allocation for Energy Storage System Considering Wind Power Distribution, IEEE Transactions on power Systems, vol. 30(2), pp. 644–52, 2015.
41. C.A. Canizares, Voltage Stability Assessment: Concepts, Practices and Tools, Power System Stability Subcommittee Special Publication IEEE/PES, thunderbox.uwaterloo.ca/∼claudio/claudio.html#VSWG, 2002.
42. F. Jabbari, B. Mohammadi Ivatloo, Static Voltage Stability Assessment Using Probabilistic Power Flow to Determine the Critical PQ Buses, Majlesi Journal of Electrical Engineering, vol. 8, pp. 17–25, 2014.
43. H. Xiong, H. Cheng, H. Li, Optimal Reactive Power Flow Incorporating Static Voltage Stability Based on Multi-Objective Adaptive Immune Algorithm, Energy Conversion and Management, vol. 49, pp. 1175–1181, 2008.
44. R. Raghunatha, R. Ramanujam, K. Parthasarathy, D. Thukaram, Optimal Static Voltage Stability Improvement Using a Numerically Stable SLP Algorithm, for Real Time Applications, International Journal of Electrical Power & Energy Systems, vol. 21, pp. 289–297, 1999.
45. X. Wang, Y. Gong, C. Jiang, Regional Carbon Emission Management Based on Probabilistic Power Flow with Correlated Stochastic Variables, IEEE Transactions on Power Systems, vol. 30, pp. 1094–1103, 2014.
46. M. Alipour, B. Mohammadi Ivatloo, K. Zare, Stochastic Risk-Constrained Short-Term Scheduling of Industrial Cogeneration Systems in the Presence of Demand Response Programs, Applied Energy, vol. 136, pp. 393–404, 2014.
47. R.D. Zimmerman, C.E. Murillo Sanchez, R.J. Thomas, MATPOWER: Steady-State Operations, Planning, and Analysis Tools for Power Systems Research and Education, IEEE Transactions on Power Systems, vol. 26, pp. 12–19, 2011.